Developing Metal Mesh Filters for Mid-Infrared Astronomy of 25 to 40 micron

Shigeyuki Sako [a], Takashi Miyata [a], Tomohiko Nakamura [a, b], Takashi Onaka [b], Yuji Ikeda [c], Hirokazu Kataza [d]

[a] Institute of Astronomy, the University of Tokyo, 2-21-1 Osawa, Mitaka, Tokyo, Japan 181-0015;
[b] Department of Astronomy, the University of Tokyo, Bunkyo-ku, Tokyo, Japan 113-0033;
[c] Photocoding, Higashi-Hashimoto, Sagamihara, Kanagawa, Japan 229-1104;
[d] Department of Infrared Astrophysics, Institute of Space and Astronautical Science, Japan Aerospace, Exploration Agency, Yoshinodai 3-1-1, Sagamihara, Kanagawa, Japan 229-8510

ABSTRACT

We have developed bandpass filters for long mid-infrared astronomy in 25 to 40μm. Most of materials become opaque in wavelengths longer than 25μm. We have applied the metal mesh method to make filters of non-transparent materials. The mesh patterns are designed based on the FDTD calculations and fabricated by the photolithography method. Measured transmittances of the fabricated filters agree with model calculations. The mesh filter has leakage in wavelengths shorter than the peak wavelength in principle. The most effective way to achieve a high stopband rejection is to stack several identical mesh filters incoherently. A narrow bandwidth fitted to atmospheric windows is required in the ground-based 30μm observations. We have fabricated a thick mesh filter without dielectric substrate, which is main source of internal absorption. The thick mesh leads to narrowing of the bandwidth due to the waveguide effect. The fabricated non-coated thick mesh filter has a peak transmittance of 0.8 and a bandwidth of $\lambda/d\lambda=8.3$ at 4 K. When stacking four of these mesh filters, it is expected to achieve a stopband rejection over 50dB, a peak transmittance of 0.41, and a bandwidth of $\lambda/d\lambda=17.5$.

Keywords: metal mesh filter, mid infrared, low temperature, photolithography, FDTD

1. INTRODUCTION

In the last several decades, infrared astronomy has developed rapidly by advancing to the space and high-altitude sites that is less affected by the earth's atmosphere. Satellites and airborne telescopes have made it possible to carry out observations in the whole infrared wavelength. While a telescope at a high-altitude site is affected by upper-air atmosphere, it has a large gain in wavelengths where water vapor is the primary cause of the atmospheric absorption. The mid-infrared, in particular longer than 20μm, is one of the wavelengths benefit from the high-altitude site. The 20μm range is accessible from sites higher than 2,000m, e.g., the Mauna Kea observatory at 4,200m altitude in Hawaii, U.S.A. and the Paranal observatory at 2,600m in Chile. The mid infrared camera and spectrograph COMICS[1, 2] mounted on the 8.2-m Subaru telescope at 4,200m has revealed spatial structures of low temperature (~ 200 K) region around young stars and late-type stars with the 24μm band filter[3]. The 20μm range is effective in observing reddened objects including highly-embedded sources and highly-redshifted sources, too. Recently, the Spitzer space telescope has achieved significant results in observing the reddened objects with the 24μm band filter, e.g., observations of embedded sources in dark clouds[4] and the PAH emissions from galaxies at $z \sim 2$[5].

Following the successes in the 20μm observations, the long mid-infrared from 25 to 40μm (LMIR) has attracted attention in recent years. The LMIR allows us to observe more reddened sources as well as a wide variety of molecular/atomic lines and dust features, e.g., the molecular lines of H_2 0-0 S(0) at 28.7μm, HD 0-0 R(2), R(3), R(4), and R(5) in the 19 to 38μm range, and OH at 34.6μm, the atomic lines of [Fe II] at 24.5, 26.0, and 35.0μm, [S I] at 25.3μm, [O IV] at 25.9μm, [S III] at 33.5μm, [Si II] at 34.8μm, and [Ne III] at 36.0μm, and the dust features of crystallized and amorphous silicates in the 18 to 34μm range. The fact that the LMIR is supported by a large format

array as a Si:Sb BIB 128 x 128 array[6] manufactured by DRS Technologies, Inc. [7] is one of the advantages. Space Infrared Telescope for Cosmology and Astrophysics (SPICA) [8] , the next generation infrared space telescope mission, places emphasis on studies in the LMIR. Atmospheric windows are opened in wavelength between 25 and 38μm at sites higher than 5,000 m. The University of Tokyo Atacama Observatory (TAO) 6.5-m telescope project[9] (PI: Yuzuru Yoshii) installed at the summit of Mt. Chajnantor at 5,640 m in Atacama, Chile plans the LMIR observations through these windows, and the University of Tokyo Atacama 1.0-m telescope[10], which is a prior project of the 6.5-m telescope, will start observations in the LMIR from 2009.

A transparent component as an optical lens is a key device for an astronomical instrument. It helps to simplify optical paths and decrease the volume. Compact design of the instrument is important especially for airborne and the space telescopes. The transmittances of materials generally used in the mid-infrared optics are shown in Figure 1. KRS5, CsI, CVD diamond and silicon have transparent characteristics in the LMIR, while most of the materials are opaque in wavelengths longer than 25μm. The LMIR transparent materials have been applied to substrates, windows and lenses in mid-infrared instruments[11, 12]. However, they are unsuitable for a dielectric interference filter, which is a general method to produce an infrared filter. The dielectric interference filter needs to stack thin layers which are formed from several different transparent materials with a high degree of accuracy. Meanwhile, KRS5 and CsI have a deliquescent and a poisonous properties, respectively. Optical properties of silicon are sensitive to crystal structure. It is not easy to grow a CVD diamond layer on the filter element. Therefore, it is difficult to fabricate the layer structure of the dielectric interference filter on the LMIR transparent materials.

A metal mesh works as a wavelength selective filter based on fundamentally different principles from the dielectric interference filter. This method utilizes electromagnetic (EM) interaction between meshed circuits and traveling EM wave. The mesh filter has been used as a frequency selective filter, a beam splitter, and a laser coupler in the far-infrared to the radio wavelengths[13, 14, 15, 16, 17]. Applications for astronomy are reviewed by Ade et al. (2006)[18]. Resonance profile and resonance frequency depend on mesh geometry and scale, respectively. Therefore, the mesh filter suffers none of the problems of the transparent material as the dielectric interference filter. In this study, we have developed LMIR band-pass filters with the metal mesh method. The LMIR mesh filter achieves a high transmittance by not using the transparent materials. In Section 2, fundamental investigation on thin mesh filters coated by polyimide will be described. In Section 3, non-coated thick mesh filters with higher transmittance and narrower bandwidth will be described.

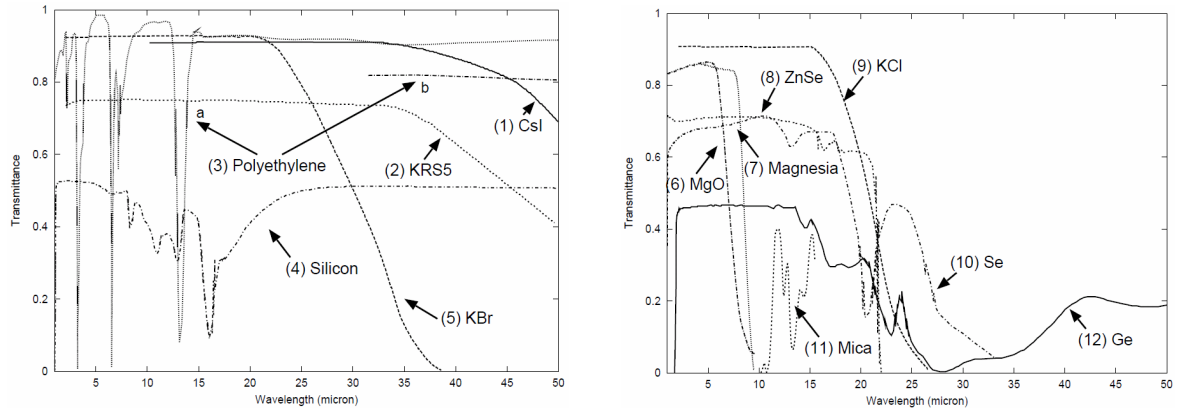

Figure 1. Transmittances of materials generally used in mid-infrared optics. (1) CsI of t = 5mm. (2) KRS-5 of t = 2 mm. (3-a) Polyethylene of t = 0.1 mm. (3-b) Polyethylene of t = 1.02 mm. (4) Silicon of t = 2 mm. (5) KBr of t = 5 mm. (6) MgO of t = 5.5 mm. (7) Magnesia of t = 10 mm. (8) ZnSe of t = 6 mm. (9) KCl of t = 10 mm. (10) Se of t = 1.69 mm. (11) Mica of t = 8μm. (12) Ge of t = 2 mm. All the data except (3) is taken from Handbook of Infrared Optical Materials[19]. The data of (3) is taken from Kiso Bussei Zuhyo (Tables of Fundamental Properties of Materials) [20].

2. COATED THIN MESH FILTER

2.1 Basic theory of cross-shaped mesh filter

The simplest metal mesh filter is formed from an orthogonal pattern of narrow wires. This type is called inductive mesh which comes from its resonance characteristics in the EM transmission line theory[21]. Geometric inverse of the inductive mesh is called capacitive mesh and has EM responses complementary to the inductive mesh based on Babinet's principle. The inductive and the capacitive meshes work as a high and a low frequency pass filters, respectively. A cross-shaped inductive mesh, shown in Figure 2[22], possesses a band pass characteristics. It can be considered as a geometric inverse of a dipole antenna array, so-called a slot antenna array, when we focus on polarized wave parallel to one arm of the cross. This means that the cross-shaped mesh has EM responses complementary to the dipole array antenna. Because a single dipole antenna has a maximum effective cross-section at the wavelength corresponding to twice the length of the dipole and a mutual resonance between the dipoles is negligible[23], the cross-shaped mesh has a bandpass characteristic as the dipole antenna. A non-polarization characteristic is obtained by placing the dipole antennas orthogonally as a cross shape. Increasing the number of the mesh elements improves total effective cross-section. The array structure produces diffraction scattering because it works as a grating element. To reduce the diffraction scattering, the crosses are placed at intervals similar to twice the resonance wavelength. Bandwidth (FWHM) of the cross-shaped mesh is $\lambda/d\lambda \sim 5$ at a maximum, which arises from the fact that a typical thin dipole antenna has a bandwidth of $\lambda/d\lambda \sim 5$. The cross-shaped mesh achieves a high stopband rejection on the longer wavelength side of the resonance peak, but it has leakage corresponding to the geometric area of the cross-shaped aperture on the shorter wavelength side in principle. Thickness of the metal mesh influences cut-on and -off profiles based on the waveguide effect, when it is not negligible relative to the resonance wavelength.

The metal mesh has been made on a transparent dielectric substrate to support refined structure of the mesh. Polypropylene and polyimide are often used as the substrate materials for the FIR to the radio wavelength filters and the MIR filters, respectively[17, 18, 24, 25]. However, the substrate materials have non-negligible absorption coefficients in the infrared, leading to reduction of the transmittance. Large refractive indices of the substrate materials also affect the transmittance characteristic because resonance condition depends on an optical path length in ambient material. Optimum mesh geometry and substrate thickness have been investigated theoretically and experientially to make a high performance filter[26, 27, 28].

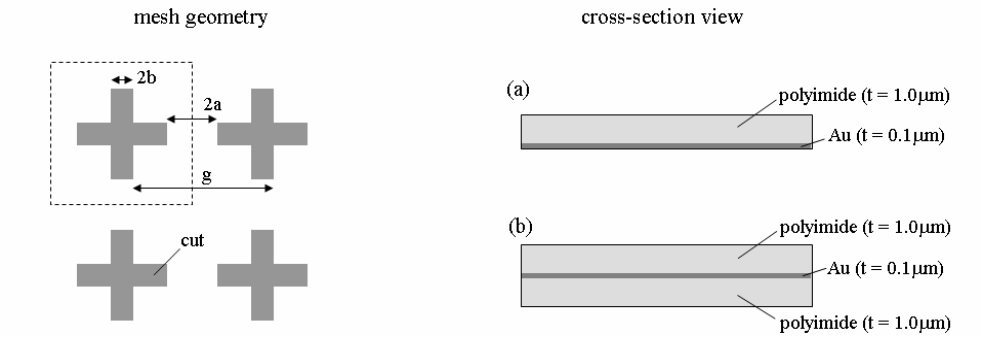

Figure 2. (*left*) Schematic of mesh geometry of the LMIR filter. A unit of the mesh pattern is indicated in a dashed rectangle. The period of the cross (**g**) is 16.8μm, the interval between the arms (**2a)** 7.0μm, and the width of the arm (**2b)** 2.7μm. The mesh is made of a thin gold film. Gray areas inside of the crosses are cut out. (*right*) Schematics of cross-section. Surface and inside of the crosses are coated and filled by polyimide. Two types of coated filter, (**a**) one-side coat and (**b**) both-sides coat, are fabricated. The thicknesses of the metal mesh and the polyimide layers are 0.1 and 1.0μm, respectively.

2.2 Design of LMIR bandpass filter

In this study, we focus on the development of a high quality LMIR bandpass filter with the cross-shaped metal mesh. A mesh geometry optimized for longer wavelengths is usable for shorter wavelengths because the peak wavelength is

simply proportional to the mesh scale. We adopt a scaled-down geometry of the 38μm bandpass filter of Smith et al. (2003) [24]. Figure 2 shows schematics of the LMIR mesh filter. The period of the cross is set to 16.8μm to adjust the peak wavelength to around 28μm. The mesh is made of a gold film of 0.1μm thickness. The mesh surface is coated by a polyimide film of 1.0μm thickness. Inside of the crosses is filled by polyimide, too. Two types of mesh filter, coated on one-side and on both-sides, are fabricated.

The refractive index of polyimide depends on individual products. We have measured wavelength dependence of the refractive index of polyimide used for the LMIR mesh filter (TORAY Semicofine SP-811) between 10 and 30μm. A polyimide film of 2.2μm thickness, formed on a silicon substrate of 2mm thickness with the spin-coat technique, is measured with a Woolam IR-VASE infrared spectral eripsometer, and the refractive index is derived with the Drude model. Figure 3 (left) shows the measured refractive index.

We have calculated EM responses of the LMIR mesh filters with the finite-difference time-domain (FDTD) method, which is a grid-based numerical modeling method with discretized time-dependent Maxwell's equations, using a commercial FDTD software RSoft FullWAVE[29]. The numerical model is composed of a cross-shaped mesh made of gold and a polyimide substrate. The refractive index of gold is taken from Ordal et al. (1983) [30]. Extrapolated values of the measured refractive index of polyimide are used for calculations in wavelengths longer than 30μm. Periodic boundary conditions are applied to the planar direction of the mesh. Polarized EM plane-wave is launched perpendicular to the mesh plane from a planar light source, and detectors for transparent and reflected EM waves are placed parallel to the mesh plane as shown in Figure 3 (right). Comparison between the transmittance calculated by the FDTD method and that measured for the fabricated product is described in Section 2.3.

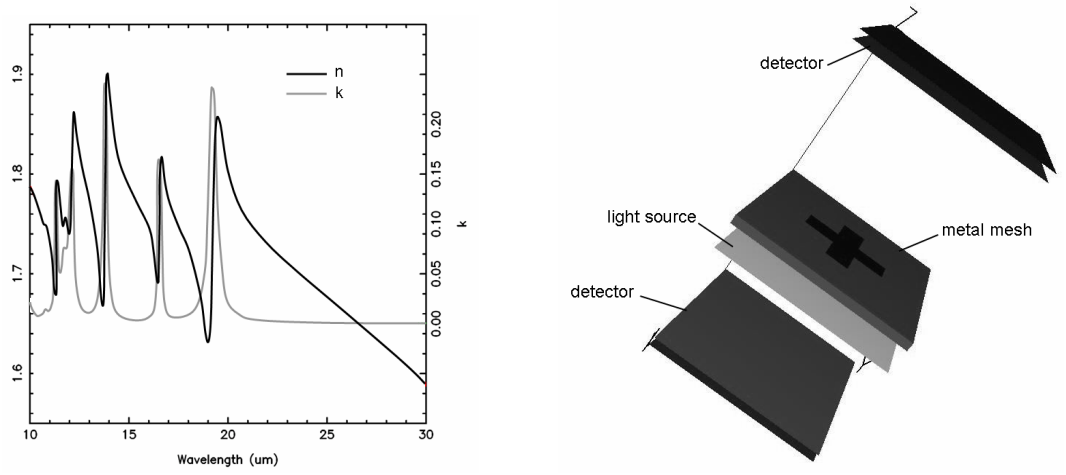

Figure 3. (*left*) Measured refractive index of polyimide used for the LMIR mesh filter (TORAY Semicofine SP-811). Solid line shows the real part of the refractive index, **n**. Gray line shows the imaginary part of the refractive index, **k**. (*right*) Numerical model of the LMIR mesh filter for the FDTD calculation.

2.3 Fabrications of LMIR bandpass filter

Fabrication method is one of the key issues for the development of the LMIR mesh filter. Submicron-scale microfabrication technique is required to produce the cross-shaped pattern of a few-μm width. It is also important to provide precise control of the thicknesses of the metal and the substrate layers. In particular, the resonance wavelength is sensitive to the substrate thickness because the effective refractive index of the substrate depends on its physical thickness when the substrate is thinner than the resonance wavelength. A production error of the substrate thickness leads to shift of the resonance wavelength.

We have fabricated the LMIR mesh filter using the photolithography technology. Initially, a thin SiO_2 layer of 500 nm thickness is formed on a polished 2 inch silicon wafer with the plasma-chemical vapor deposition (P-CVD) method. This layer is removed by etching with hydrofluoric acid (HF) to exfoliate the filter element from the silicon wafer at the end

of the process. Polyimide is placed on the surface by the spin-coating technique and then is cured. UV photopatterning is performed using the two-layer photoregist method. Scanning electron microscopy (SEM) images of photopattern at the center portion of the wafer are shown in Figures 4a and b. The corner radii of the crosses are about 0.1 and 0.5μm at the center and the edge of the wafer, respectively. A titanium film of 10nm thickness and a gold film of 0.1μm thickness are then deposited onto the surface by the metal evaporation method. Figures 4c and d show SEM images of the deposited metal surface at the center portion of the wafer. The metal surface is smooth without bumps nor dips. In one of the two processes, the polyimide layers are formed on the both sides as described in Figure 2 (right). The wafers are divided into five square pieces of 16 mm on a side by a dicing saw. Finally, the filter elements are exfoliated from the silicon wafers by immersion in a dilute HF bath. Local geometry of the filter element is kept constant even after exfoliation, but global geometry is wrinkled as shown in Figure 4e. Discrepancies between the design and the product are about 0.1μm (~1%) in the length of the single cross, **g-2a** and about 0.03μm (~30%) and 0.1μm (~8%) in the thicknesses of the metal and the polyimide layers, respectively. The thicknesses of the layers are measured with SEM images taken after the filter elements are cut by a focused ion beam (FIB).

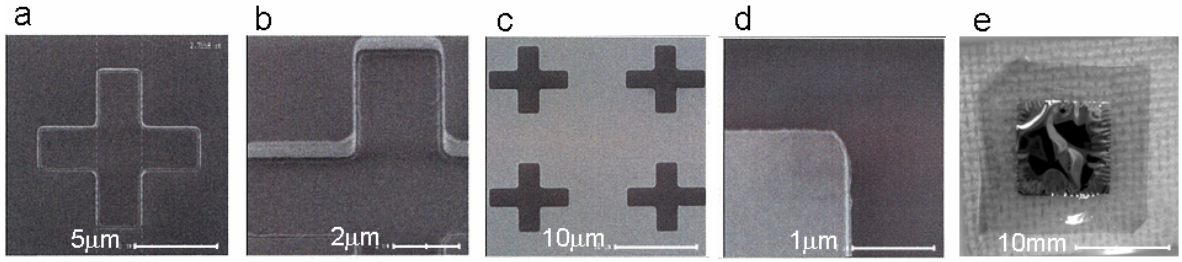

Figure 4. (**a**) SEM image of photopattern at the center portion of the wafer. (**b**) Tilted image of (**a**). (**c**) SEM image of the deposited metal surface at the center portion of the wafer. (**d**) Tilted image of (**c**). (**e**) Overview image of the LMIR mesh filter. The metal mesh is in the inner 10 mm square. Surrounding area is made of a polyimide film. The scales of the images are shown at the bottom.

2.4 Measurements of transmittance

We have measured transmittances of the fabricated LMIR mesh filters between 200 and 5,000 cm^{-1} (2 to 50μm) using a Fourier transform spectrometer Bruker IFS 125/HR[31] at Department of Astronomy, the University of Tokyo. The mesh filter is fixed in an aluminum holder of 10 mm aperture, and then set in a continuous flow helium cryostat Oxford Optistat CF-V. The transmittances are measured with a 5 mm beam through KRS-5 windows at the room temperature. A Mylar beam splitter of 6μm thickness and a deuterated L-alanine doped triglycene sulphate (DLATGS) pyroelectric detector are used.

The measured transmittances are plotted in Figure 5. Single peaks of the transmittances are seen at 24 and 29μm in the data of the one-side and the both-sides coated filters, respectively. In wavelengths shorter than 20μm and longer than 40μm, the transmittance data is noisy due to the characteristics of the beam splitter and the detector. Absolute accuracies of the transmittances are less than 5% except in the noisy wavelengths. There is leakage of a few percent in wavelengths shorter than the resonance wavelength, which is one of the principle characteristics of the mesh filter as described in Section 2.1.

Results of the FDTD calculations are superimposed on the measured data in Figure 5 (left). The constant refractive index of (n, k) = (1.6, 0.01) from our measurements is applied to the numerical models of the polyimide layers. The FDTD calculations reproduce the measured profiles and the peak wavelengths well, but the calculated peak intensities are about 15 and 30% different from the measurements of the one-side and the both-sides coated filters, respectively. Discrepancies of the peak wavelengths (~ 1 %) are explained by the production error of the cross-shaped geometry, while those of the peak intensities might be caused by the fact that the numerical modeling of refractive index distribution is inappropriate and/or the filter elements are wrinkled across the whole area. The measured transmittances are reproduced by the FDTD calculations using a refractive index k of 0.05 for polyimide as shown in Figure 5 (right). This means that excess absorption arises in the polyimide layers, but production mechanism of the excess absorption is unclear at the moment. The first order diffractions due to the grating effect of the mesh pattern are seen as the second

peaks around 15μm in the FDTD calculations. Since the diffracted light is propagated outside of the detector, the second peaks do not appear in the measured transmittances.

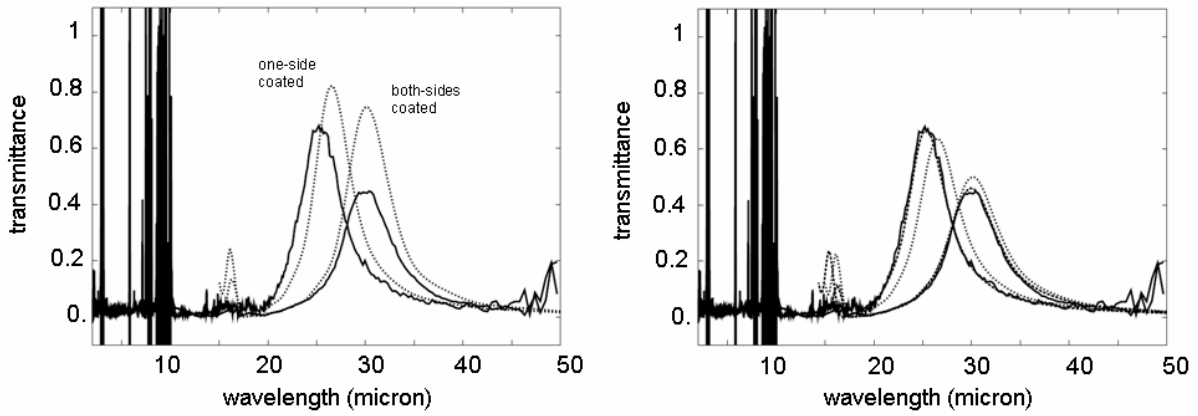

Figure 5. (*left*) Measured and calculated transmittances of the LMIR mesh filters. The measurement data is plotted in solid lines. Transmittance peaks of the one-side and the both-sides coated filters are seen at 24 and 29μm, respectively. Dotted lines show results of the FDTD calculations. (*right*) Numerical models reproducing the measured transmittances. Solid lines show the measurement data. Dotted lines show results of the FDTD calculations with a refractive index k of 0.05. Dashed lines show fitted model profiles, which are produced by scaling up and down the profiles calculated with k = 0.05. For the one-side coated filter, the wavelength and the transmittance coordinates are reduced by 4.5 percent and expanded by 5 percent, respectively. For the both-sides coated filter, the wavelength and the transmittance coordinates are reduced by 0.5 and 8 percents, respectively.

3. NON-COATED THICK MESH FILTER

3.1 Design of non-coated thick mesh filter

Stopband rejection over 50 dB (0.001 %) is required for a band-pass filter in astronomical observations. However, the mesh filter has leakage of a few percent in wavelengths shorter than the resonance peak in principle. While absorption material works as a blocking filter, it is difficult to use it as a short wavelength cut filter as most of the materials have larger absorption coefficient in longer wavelengths. The most effective way to achieve the high stopband rejection is to stack several identical mesh filters incoherently. In this instance, peak transmittance of a single mesh filter is required to be close to unity.

As discussed in Section 2.4, the polyimide layers are major sources of the internal absorption. Results of the FDTD calculations for a non-coated mesh filter are presented together with those of the coated filters in Figure 6 (left). The non-coated filter has the same mesh geometry as those of the coated filters. A constant refractive index of (n, k) = (1.6, 0.05) is applied to the models of the polyimide layers. As the polyimide layer becomes thinner, the peak wavelength shifts shortward and the peak intensity increases. Maximum peak intensity is achieved when the metal mesh is not coated. The bandwidth also depends on the thickness of the polyimide layer. The non-coated filter has a narrower bandwidth of $\lambda/d\lambda$=6.3 than those of the coated filters. The results of the FDTD calculations demonstrate that the non-coated filter has a high efficiency and is suited for making the stacked mesh filter.

One of aims of this study is to develop band-pass filters for the ground based 30μm observations. There are several atmospheric windows, whose widths are 2 to 3μm, in the 30μm range at the TAO site (5,640m) [10]. Medium band-pass filters of $\lambda/d\lambda$=10–15 are necessary to perform high sensitivity observations through these atmospheric windows. A thick mesh filter is expected to produce a narrower bandwidth and sharper cut-on and -off transitions because the thick metal mesh produces the waveguide effect when the metal thickness is not negligible relative to the resonance wavelength[32]. Results of the FDTD calculations for non-coated thick mesh filters are shown in Figure 6 (right). The filters have the same mesh geometry as those of the coated filters. As the metal layer becomes thicker, the peak wavelength shifts shortward and the bandwidth becomes narrower. When the metal layer is thicker than 1.0μm, the peak intensity starts to

get diminished. The bandwidth is calculated to be λ/dλ=8.5 for the 1.0μm thickness filter. The thick mesh filters achieve higher stopband rejection than the thin filters on the longer wavelength side of the resonance peak. The results of the FDTD calculations demonstrate that the non-coated thick mesh filter is suitable for the ground based 30μm observations. The waveguide effect depends on the scale of the mesh structure as the cross-dipole array effect. To design the thick mesh filter for the longer LMIR, it is needed to increase the metal thickness in proportion to the resonance wavelength.

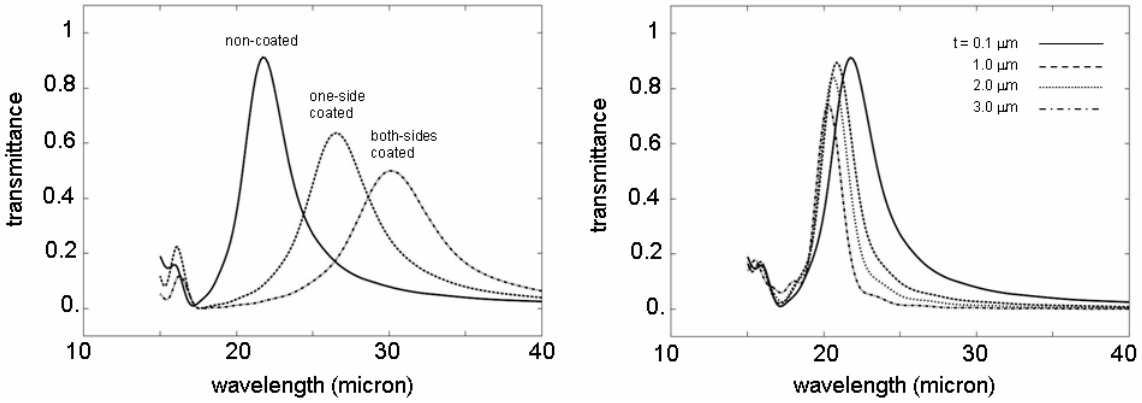

Figure 6. (*left*) Comparison between results of the FDTD calculations for a non-coated filter and polyimide coated filters. Solid line shows transmittance of the non-coated filter, while dashed and dashed-dotted lines show those of the one-side and the both-sides coated filters, respectively. The non-coated filter has the same mesh geometry as those of the coated filters. The polyimide thickness on each side is 1.0μm. A refractive index of k =0.05 is used for the polyimide model. The metal thicknesses of all the models are 0.1μm. The bandwidths are λ/dλ=4.8, 5.2, and 6.3 for the non-coated, the one-side coated, and the both-sides coated filters, respectively. (*right*) Results of the FDTD calculations for non-coated thick mesh filters. Solid, dashed, dotted, and dashed-dotted lines show transmittance profiles when the metal thicknesses are 0.1, 1.0, 2.0, and 4.0μm, respectively. The non-coated thick filters have the same mesh geometry as those of the coated filters. The bandwidths are λ/dλ=6.3, 8.5, 9.7, and 10.6, respectively.

3.2 Fabrications and evaluations of non-coated thick mesh filter

We have fabricated the non-coated mesh filter of 1.0μm thickness with the same method as the coated mesh filters. The non-coated mesh, which is made of only a gold film, is very fragile. A silicon ring of 10 mm aperture is used as a supporting frame for the mesh structure. It is bonded on the metal mesh layer by using a photoregist as glue before the filter element is exfoliated from the silicon wafer. An overview picture of the non-coated thick mesh filter is shown in Figure 7 (left). The fixed mesh filter has a smooth surface without wrinkles.

The transmittances of the fabricated non-coated thick mesh filter are measured at the room temperature and 4 K using the same instruments used in Section 2.4. The filter piece is cooled by liquid helium in the cryostat. As LMIR filters are generally used at temperatures lower than 30 K, it is important to evaluate the mesh filter at the low temperatures. The measured transmittances are plotted in Figure 7 (right). The fabricated non-coated mesh filter achieve a high peak transmittance of 0.8 and a narrow bandwidth of λ/dλ=8.3 at 4 K. The fixed filter element is not damaged by a single cooling cycle, and the transmittance profile is unchanged before and after the cooling cycle. Further cooling tests are necessary to verify low temperature durability of the filter piece. While the peak wavelength of the transmittance is unchanged between the room temperature and 4 K, the peak transmittance shows drastic change at temperatures between 200K and 80K, resulting in an increase by 10% at 4K. The variation of the peak transmittance should not be caused by thermal expansion of the metal mesh or the silicon frame because the peak wavelength is not shifted. Temperature dependence of electric resistance on the mesh surface is more likely. To resolve the mechanism of the amplification at the low temperatures, cooling tests for various kinds of mesh filter are necessary.

Results of the FDTD calculations for the non-coated thick mesh filter are represented together with the measured data in Figure 7 (right). The FDTD calculations reproduce the measurements well. The peak intensities measured at 300K and 4K differ from that of the simulated profile by about 20 and 10%, respectively. The measured peak wavelengths are about 5% different from the simulation. The transmittance profile measured at 4 K is well fitted by scaling down the

results of the FDTD calculations by 5 and 10% for the wavelength and the transmittance coordinates, respectively, as shown in Figure 7 (right).

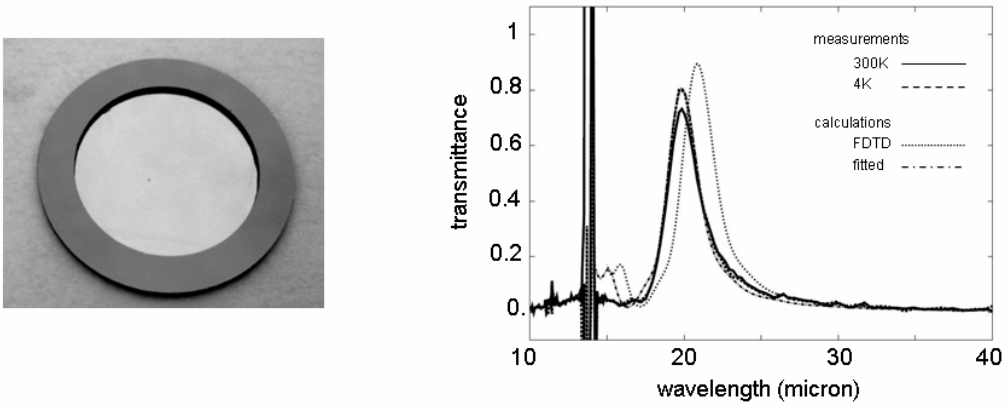

Figure 7. (*left*) Overview picture of a non-coated thick mesh filter. The filter element is fixed in a silicon ring of 10 mm aperture and about 400μm thickness. (*right*) Transmittances of the fabricated mesh filter and results of the FDTD calculations. Solid and dashed lines show transmittances of the fabricated non-coated thick mesh filter measured at the room temperature and 4 K, respectively. Dotted line shows result of the FDTD calculations for the non-coated thick mesh filter. Dashed-dotted line shows a numerical model reproducing the transmittance profile at 4 K. This profile is produced by scaling down the result of the FDTD calculations by 5 and 10% for the wavelength and the transmittance coordinates, respectively. The bandwidth of the non-coated thick mesh filter at 4 K is $\lambda/d\lambda$=8.3.

3.3 Stacked mesh filter

The most effective way to achieve a high stopband rejection over 50 dB is to stack several identical mesh filters incoherently. When two identical filters are set parallel to each other, total transmittance is expressed as

$$T_{total}(\lambda) = \frac{T(\lambda)}{2 - T(\lambda)}, \quad (1)$$

where $T(\lambda)$ is a transmittance of a single filter in a wavelength of λ, and loss-free reflection is assumed. The gain obtained by the stacking is not remarkable due to internal reflection between the two filters. This problem is resolved by tilting the second filter by a few degree. An optical filter is usually placed near a pupil position and a beam passing the filter is focused on a detector array by camera optics in a general astronomical infrared instrument. When the tilt angle is sufficient, components of the internal reflection are focused out of the array. In the MAX38 mid infrared camera[11] for the University of Tokyo Atacama 1.0-m telescope, tilt angles of more than 3 degree are required. The tilted mesh filter produces polarization because apparent lengths of the crosses arm is shrunk in the tilted direction. This affect is reduced by tilting the first filter in the direction orthogonal to that of the second filter. When the mesh filters are placed at appropriate tilt angles, the stacked mesh filter is expected to produce total transmittance expressed as

$$T_{total}(\lambda) = T(\lambda)^n, \quad (1)$$

where n is the number of stacked filters. To achieve the stopband rejection of 50 dB, it necessary to stack at least four mesh filters. Figure 8 shows an expected transmittance profile of a four-layer-stacked mesh filter which is produced by raising the transmittance of the non-coated thick mesh filter at 4 K to the fourth power. The peak transmittance and the bandwidth of the stacked filter are 0.41 and $\lambda/d\lambda$=17.5, respectively.

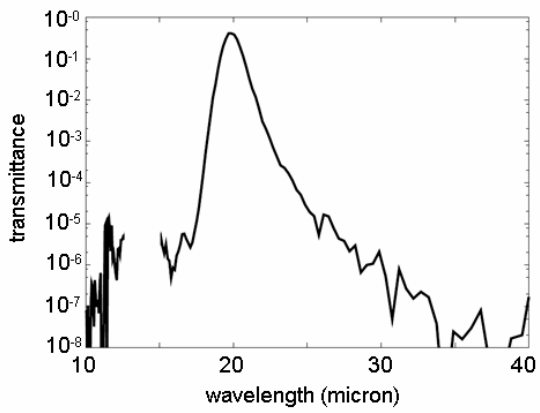

Figure 8. Expected transmittance profile of a four-layer-stacked mesh filter. It is produced by raising the transmittance of the non-coated thick mesh filter at 4 K to the fourth power. The profile in wavelength between 12.5 and 15μm is masked because the 4K measurement data is noisy. The peak transmittance and the bandwidth of the stacked filter are 0.41 and $\lambda/d\lambda$=17.5, respectively.

4. SUMMARY

We have developed bandpass filters for long mid-infrared (LMIR) astronomy in 25 to 40μm. The metal mesh method is applied to make filters of non-transparent materials. Mesh patterns are designed based on the FDTD calculations. The refractive index of polyimide used for filter substrate is measured for the FDTD calculations. We fabricate cross-shaped mesh filters coated by polyimide using the photolithography method. Discrepancy between the design and the product is about 0.1μm (~1%) in the length of the cross, and about 0.03μm (~30%) and 0.1μm (~8%) in the thicknesses of the metal and the polyimide layers, respectively. The corner radii of the metal patterns are about 0.1 and 0.5μm at the center and the edge of the wafer, respectively. Measured transmittances of the fabricated filters agree with the model calculations. The FDTD calculations demonstrate that the polyimide layers are main sources of internal absorption in the mesh filter.

The mesh filter has leakage in wavelengths shorter than the peak wavelength in principle. The most effective way to achieve a high stopband rejection over 50 dB (0.001 %), required in astronomical observations, is to stack several identical filters incoherently. To make a high efficient stacked filter, the peak transmittance of the single filter is required to be closed to unity. The FDTD calculations indicate that a non-coated mesh filter has a higher transmittance than those of the coated filters. To perform high sensitivity observations in the 30μm from ground, narrowband filters fitted to atmospheric windows are required. A thick mesh filter is expected to produce a narrower bandwidth and shaper cut-on and -off transitions because it produces the waveguide effect. We fabricate a non-coated thick mesh filter of 1.0μm thickness and measure the transmittance at the room temperature and 4 K. The fabricated non-coated thick mesh filter has a peak transmittance of 0.8 and a bandwidth of $\lambda/d\lambda$=8.3 at 4 K. The filter piece is not broken by a single cooling cycle. When stacking the four mesh filters, it is expected to achieve a stopband rejection over 50 dB, a peak transmittance of 0.41, and a bandwidth of $\lambda/d\lambda$=17.5.

This research was supported by Ministry of Education, Culture, Sports, Science, and Technology of Japan, Grant-in-Aid for Scientific Research (grant no. 18740098), National Astronomical Observatory of Japan, Research Grant for Joint-development, and Japan Aerospace Exploration Agency. We are grateful to all of the staff members of the TAO project and the SPICA project, and to Dr. Itsuki Sakon of the University of Tokyo for his helpful support for the measurements of the filters. S. S. is financially supported by the Japan Society for the Promotion of Science (18-9936).

REFERENCES

[1] Kataza, H., et al., "COMICS: The Cooled Mid-Infrared Camera and Spectrometer for the Subaru Telescope," Proc. SPIE 4008, 1144-1152 (2000).

[2] Okamoto, Y. K., et al., "Improved performances and capabilities of the cooled mid-infrared camera and spectrometer (COMICS) for the Subaru telescope", Proc. SPIE 4841, 169-180 (2003).

[3] Fujiwara, H., et al., "The Asymmetric Thermal Emission of the Protoplanetary Disk Surrounding HD 142527 Seen by Subaru/COMICS," ApJ, 644L, 2, 133-136 (2006)

[4] Young, C. H., et al., "A ``Starless'' Core that Isn't: Detection of a Source in the L1014 Dense Core with the Spitzer Space Telescope," ApJS, 154, 1, 396-401 (2004)

[5] Reddy, N. A., et al., "Star Formation and Extinction in Redshift z~2 Galaxies: Inferences from Spitzer MIPS Observation," ApJ, 644, 2, 792-812 (2006)

[6] Hogue, H. H., et al., "Space mid-IR detectors from DRS," Proc. SPIE 4850, 880-889 (2003).

[7] WWW home of DRS Technologies, Inc; http://www.drs.com/

[8] Onaka, T., et al., "Development of large aperture cooled telescopes for the space infrared telescope for cosmology and astrophysics (SPICA) mission," Proc. SPIE 5962, 448-462 (2005).

[9] Yoshii, Y. et al., "Tokyo Atacama Observatory Project", Proc. IAU 8th Asian-Pacific Regional Meeting, VolII, eds. Ikeuchi S., Hearnshaw J., Hanawa T., 35-36 (2002)

[10] Sako, S. et al., "The University of Tokyo Atacama 1.0-m Telescope," in this conference.

[11] Miyata, T. et al., "A new midinfared camera for ground-based 30 micron observations: MAX38," in this conference.

[12] Onaka, T., et al., "The Infrared Camera (IRC) for AKARI -- Design and Imaging Performance," PASJ, 59, 2, 401-410 (2007)

[13] Nolte, D. D. and Richards, P. L., "Far-infrared dichroic bandpass filters," Applied Optics, 24, 10, 1541-1545 (1985)

[14] Bock, J. J., et al., "Silicon-gap Fabry-Perot filter for far-infrared wavelengths," Applied Optics, 34, 19, 3651-3657 (1995)

[15] Möller, K. D., et al., "Capacitive-grid beam splitters for far-infrared and millimeter-wave interferometers," Applied Optics, 23, 18, 3075-3078 (1984)

[16] Dragovan, M., "Cryogenic metal mesh bandpass filters for submillimeter astronomy," Applied Optics, 23, 16, 2798-2802 (1984)

[17] Irimajiri, T. and Takano, T., "Frequency Selective Surfaces for Radio Astronomy," Experimental Astronomy, 2, 123-136 (1991)

[18] Ade, P. A. R., et al., "A Review of Metal Mesh Filters," Proc. SPIE 6275, 62750U1- 62750U15 (2006).

[19] Klocek, P., "Handbook of Infrared Optical Materials" Marcel. Dekker, New York (1991)

[20] Kudo, K., "Kiso Bussei Zuhyo (Tables of Fundamental Properties of Materials) " Kyoritsu Shuppan, Tokyo (1972)

[21] Ulrich, R., "Far-Infrared Properties of Metallic Mesh and its Complementary Structure, " Infrared Physics, 7, 37-55 (1967)

[22] Ulrich, R., "Interference filters for the far infrared," Applied Optics, 7, 1987-1996 (1968)

[23] Wickersham, A. F., Jr, "Anomalous Dispersion in Artificial Dielectrics," Journal of Applied Physics, 29, 11, 1537-1542 (1958)

[24] Smith, H. A. et al., "Designer infrared filters using stacked metal lattices, " Applied Physical Letters, 82, 21, 3605-3607 (2003)

[25] Lüker, A. et al., "Thick capacitive meshes on polyimide substrates," Infrared Physics and Technology, 45, 153-157 (2004)

[26] Whitbourn, L. B. And Compton, R. C., "Equivalent-circuit formulas for metal grid reflectors at a dielectric boundary," Applied Optics, 24, 2, 217-220 (1985)

[27] Möller, K. D. and Sternberg, O., "Thick inductive cross shaped metal meshes," Journal of Applied Physics, 91, 12, 9461-3926 (2002)

[28] Möller, K. D. et al., "Inductive cross-shaped metal meshes and dielectrics," Applied Optics, 41, 19, 3919- (2003)

[29] WWW home of RSoft, Inc; http://www.rsoftdesign.com/

[30] Ordal, M. A., et al., "Optical properties of the metals Al, Co, Cu, Au, Fe, Pb, Ni, Pd, Pt, Ag, Ti, and W in the infrared and far infrared," Applied Optics, 22, 7, 1099-1120 (1983)

[31] WWW home of Bruker Optics, http://www.brukeroptics.com/

[32] Winnewisser, C. et al., "Transmission features of frequency-selective components in the far infrared determined by terahertz time-domain spectroscopy," Applied Optics, 38, 18, 3961-3967 (1999)